Journal of Thermal Analysis and Calorimetry (2026) 151:2141–2156
https://doi.org/10.1007/s10973-025-15196-3

The synergistic effect of expandable graphite and zinc oxide as flame retardants on the properties of epoxy resin

Péter Csvila[1] · Zsófia Kovács[1,2] · Andrea Toldy[1,2] · Tibor Czigany[1,3]

Received: 14 May 2025 / Accepted: 6 December 2025 / Published online: 13 January 2026
© The Author(s) 2026

Abstract

In this study, zinc oxide (ZnO) nanoparticles and expandable graphite (EG) were used as flame retardants to reduce the flammability of epoxy resin. The flame retardants increased the flexural modulus of the epoxy matrix by up to 50%. The effective heat of combustion of the samples containing both ZnO and EG was reduced to more than one-third of the reference value, while the maximum average rate of heat emission of the samples showed a reduction of almost 60% compared to pure epoxy. During the burning of the epoxy resin, ZnO and EG reduced the emission of gas-phase compounds containing C–H and N–H bonds. The incorporation of ZnO into the epoxy matrix resulted in a "puff pastry-like" structure that facilitated the release of evolved gases during combustion, thereby promoting foaming in the intumescent char formation process. Moreover, ZnO contributed to the enhanced structural stability of the EG residue.

Graphical Abstract

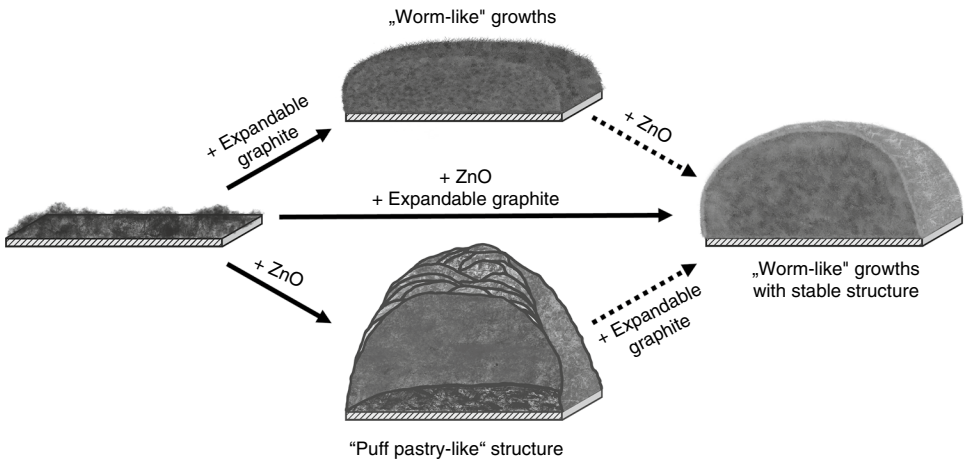

Keywords Flame retardancy · Expandable graphite · Zinc oxide · Epoxy resin · Residual structure

Introduction

In polymer technology, especially in the composites industry, thermoset materials such as epoxy resins are widely used. These epoxy matrix-based composite products can be found, for example, in the aeronautics (wings), the energy (wind turbines), and the building industry (facade panels). Generally, epoxy resins have good strength, excellent chemical resistance, and favorable mechanical properties. In addition, they can provide excellent adhesion to various fillers and reinforcing materials such as carbon fibers, glass fibers, or ceramic fillers [1]. However, during the burning of epoxy resins, high amount of heat and smoke are produced, which cause health and safety risks [2]. Due to the cross-linked structure of epoxy resins, complex thermal decomposition processes occur during burning. Their burning properties are strongly influenced by their chemical structure and

Extended author information available on the last page of the article

the way they are produced. Therefore, burning intensity, heat release, and the gases and smoke released during burning can be different for different epoxy resins. For example, burning epoxy resins can release carbon dioxide (CO_2), carbon monoxide (CO), water vapor (H_2O), nitrogen-containing gases, and other organic compounds that can be harmful to health [3, 4]. In addition to the release of toxic gases, the high rate of heat release during combustion contributes to rapid fire growth, emphasizing the need for flame-retardant systems [5].

Intumescent flame retardants play a significant role in the flame retardancy of polymers. They have been extensively studied [6–8], as they greatly influence the flammability parameters of polymers. They can significantly reduce smoke emissions and the release of hazardous gases into the environment and even prevent the dripping of polymers. Intumescent flame retardants form a protective, expanded char layer on the surface of the polymer upon heating, as a result of gas release and charring reactions triggered by thermal decomposition. Intumescent flame retardants can retard further thermal degradation and the burning of polymers, which is why this type of mechanism is used in automotive, construction, and even electronics applications. Typically, intumescent systems contain three main components: an acid source, a char-forming agent, and a blowing agent, which form the protective layer together. Examples of such typical intumescent flame-retardant ingredients include ammonium polyphosphate (APP), which is the acid source containing phosphorus, pentaerythritol (PER), which acts as a char-forming compound, and melamine (MEL), which is the foaming agent [9, 10].

Inorganic flame retardants, such as metal oxides, are also used in the flame retardation of polymers. In many cases [11, 12], metal oxides improve the stability of the resulting char layer and positively affect the thermal stability of the polymer matrix. In addition to increasing thermal stability, metal oxides can also accelerate the formation of the protective char layer by catalyzing thermal degradation [13]. Commonly used inorganic flame retardants include titanium dioxide, aluminum oxide, and zinc oxide (ZnO) [14]. In addition to increasing the stability of the burn residue, these materials can also improve the insulating properties of the protective char layer, limiting the further burning of the polymer material and the emission of combustion gases. Inorganic flame retardants also include metal hydroxides, which have the advantage of not producing compounds which damage health, the environment or are corrosive. Furthermore, their decomposition is an endothermic process, which removes heat from the burning environment. In addition, during the burning process, water is produced by metal hydroxides in the form of water vapor, which makes it difficult for oxygen to reach the burning surface [15]. However, despite their favorable flame-retardant properties, their disadvantage is that they are only effective in higher mass percentages. In addition, high loading levels affect the mechanical properties of the matrix. For example, the addition of APP reduces tensile and flexural strength, but improves impact strength [16]. In the case of metal hydroxides, such as magnesium hydroxide, a similar effect can be observed: In high mass percentages, they effectively improve flame retardancy, but significantly reduce mechanical properties such as tensile strength and elongation at break [17].

Other nano- or microscale inorganic materials are also often used as flame retardants, such as carbon nanotubes and graphene [18], montmorillonite [19], or even expandable graphite (EG) [20]. EG expands at high temperatures. This expansion is caused by the redox reaction of the graphite and an acid source, such as sulfuric acid (H_2SO_4), which is incorporated between the graphite layers. The resulting burning products create an insulating protective layer that prevents the further oxidation of the lower polymer layer. The reaction is typically activated above 200 °C, and a protective layer of a "worm-like" structure is produced, which prevents the transfer of heat and mass between the polymer and the heat source [21]. Furthermore, the nanoparticles can diffuse to the burning surface during burning, creating a protective layer on the polymer surface and preventing heat and mass transfer [22]. The advantage of nanoscale flame retardants over metal hydroxides is that, with proper dispersion, they can even improve the mechanical properties of the base polymer, such as tensile strength and modulus, but with poor dispersion, mechanical properties can also decrease [23].

Adding flame retardants often changes the color of the original polymer matrix. For example, red phosphorus turns the polymer red (burgundy) [24], and EG turns the polymer dark gray. Metal oxides (such as magnesium oxide or zinc oxide) color the polymer white. In many cases, the color of the polymer product is also important. May et al. [25] reported that painting polymer composite wind turbine blades black can reduce the crash rate of birds into wind turbines by up to 70%. By coloring the resin in its material, composite products can be colored in one step.

Our goal was to develop an epoxy resin matrix material where the flame-retardant additives provide both safety functions and colors. The purpose is to develop a flame-retardant matrix that is grayish-black in color and, if it burns, releases less heat, and produces fewer toxic gases. For this purpose, ZnO and EG were added to the epoxy resin in different concentrations to improve its thermal properties and color it.

Materials and methods

Materials

The matrix material was an epoxy resin, which was prepared by mixing the pentaerythritol-based IPOX MR

3016 (Ipox Chemicals Ltd., Hungary) monomer with the cycloaliphatic amine-based IPOX MH 3124 (Ipox Chemicals Ltd., Hungary) cross-linking agent. The epoxy monomer and cross-linking agent were mixed in a mass ratio of 100:40. Commercial zinc oxide particles (ZnO, Molar Chemicals Kft., Hungary) were used in different mass percentages (10 mass%, 20 mass%, and 30 mass%) without any surface and chemical treatment. Median particle size was 0.795 µm, and 90% of the particles were below 2.88 µm. EG ES100 C10 expandable graphite (EG, Graphit Kropfmühl, Germany) was used in two different concentrations (5 mass% and 10 mass%) to improve flame retardancy. Seventy-five percent of the particles were below 150 µm, and their expansion rate was 100 $cm^3\ g^{-1}$.

Table 1 Tested samples and their additive content

Sample	ZnO content/ mass%	EG content/ mass%
Z0-G0	0	0
Z10-G0	10	0
Z20-G0	20	0
Z30-G0	30	0
Z0-G5	0	5
Z10-G5	10	5
Z20-G5	20	5
Z30-G5	30	5
Z0-G10	0	10
Z10-G10	10	10
Z20-G10	20	10
Z30-G10	30	10

Preparation of the flame-retardant epoxy matrices

In the first step, the particles (ZnO, EG) were mixed into the epoxy matrix monomer. During mixing, the particles were first dispersed by mechanical stirring for 5 min, and then, ultrasonic homogenization was applied for 3 min to improve the homogeneous dispersion of the particles. A Bandelin Sonopuls 4200 HD UH homogenizer (BANDELIN Electronic GmbH & Co. KG, Germany) was used for ultrasonic stirring, with a power of 100 W and a frequency of 20 kHz. During homogenization, the temperature of the suspension was kept below 60 °C with a cooling bath. After dispersing the flame-retardant particles, we added the cross-linking agent to the epoxy monomer (in a mass ratio of 100:40) and then poured it into a mold of the appropriate size for the measurements. The epoxy resin test specimens were cured at 80 °C for 1 h, then post-cured at 100 °C for 1 h. Flame-retarded samples were labeled Zxx-Gxx, where Z refers to ZnO content, the number (xx) behind it indicates the amount of ZnO, G refers to EG, and the number (xx) behind it indicates the amount of EG in mass percentage (mass%). Table 1 summarizes the test specimens and the quantity of particles in them.

Testing and characterization

Thermogravimetric analysis (TGA)

The thermal stability of the samples was determined with a TA Instruments Q500 thermogravimetric analyzer (TGA, New Castle, DE, USA). The sample masses were between 5 and 10 mg. The test was carried out in both nitrogen and air atmosphere. The flow rate was 30 mL min^{-1}, the heating rate was 20 °C min^{-1}, and the temperature range was 30–600 °C.

Table 2 Classifications and criteria for the UL-94 test

Criteria	V-0	V-1	V-2
Burn time after ignition	≤10 s	≤30 s	≤30 s
Ignition, smoke production time after the second ignition	≤30 s	≤60 s	≤60 s
Total ignition time	≤50 s	≤250 s	≤250 s
Can cotton wool be ignited?	no	no	yes
Is the test piece touching the end?	no	no	no

(Based on ISO 9772 and ISO 9773 standards)

UL-94 flammability test

The UL-94 flammability tests were carried out according to the ISO 9772 and the ISO 9773 standards on 120 mm × 10 mm × 4 mm samples. The flame spread rate was determined from horizontal (H) tests, and the classification of flame retardancy from vertical (V) tests. A sample was rated HB if it reached the first mark on the horizontal test and burned slower than 40 mm min^{-1}. Table 2 shows the V classification types of vertical tests and their criteria.

Limiting oxygen index (LOI)

Limiting oxygen index (LOI) tests were performed according to ISO 4589–1 and ISO 4589–2 on 120 mm × 10 mm × 4 mm samples. The oxygen index was the minimum oxygen volume percentage (volume%) that could still maintain burning in an oxygen–nitrogen gas mixture at a given flow rate.

Mass loss type cone calorimetry (MLC)

The complex combustion characteristics of the samples were determined with a mass loss type cone calorimeter

(MLC, Fire Testing Technology, UK). The tested samples were nonstandard, with a size of 40 mm × 40 mm × 4 mm, and a heat flux of 25 kW m^{-2} was applied due to their intense foaming. The measured results were converted to 100 mm × 10 mm × 4 mm standard specimens with a proportional method. During the tests, a spark ignition unit was used to ignite the specimen surfaces. We determined time to ignition (TTI), total heat release (THR), peak heat release rate (pHRR), time to pHRR and residual mass, and also the maximum average rate of heat emission (MARHE) and the effective heat of combustion (EHC). MARHE is the average amount of heat released during combustion and indicates the overall flammability of the material. EHC is the amount of heat released per unit mass of the material during combustion. The MARHE and EHC values are used to evaluate the solid- or gas-phase action of the flame retardants [26].

Laser pyrolysis–Fourier transform infrared spectrometry (LP-FTIR)

The gases emitted during the burning of the samples were tested with a SYNRAD 48–1 variable power CO_2 laser (Novanta Inc., USA) and analyzed with the Bruker Tensor 37 FTIR spectrometer (Bruker, USA). In each case, the samples were pyrolyzed for 60 s with a power of 1 W, and the released gases were detected. Sample size was 20 mm × 10 mm × 4 mm.

Analysis of the residual structure and visual properties

The structure of the residual material after burning was characterized with a Keyence VHX-5000 optical microscope (Keyence Corporation, Belgium). The composition of the residues after burning was determined with an SEM JEOL JSM 6380LA scanning electron microscope (Jeol Ltd., Japan). The surface of the samples was made conductive with a Jeol JPC1200 cathodic powder gold coating device (Jeol Ltd., Japan) to avoid charging. The particle distribution of the burned residues was mapped by scanning electron microscopy and energy-dispersive spectrometry (SEM–EDS) at 500 × magnification.

The color of the samples was analyzed from scanned images. After the images were captured, they were analyzed pixel by pixel with MATLAB. The analysis determined the individual RGB color code of each pixel and then determined the average color of the sample for the whole image, which gave the average RGB value. The grayscale value was determined from the RGB values according to (1) [27]:

$$Y = 0.2126 \bullet R + 0.7152 \bullet G + 0.0722 \bullet B \quad (1)$$

where Y is the average grayscale value for the sample, R is the average red color value, G is the average green color value, and B is the average blue color value.

Mechanical properties

The mechanical tests were carried out on a Zwick Z005 tensile testing machine (Zwick GmbH & Co. KG, Germany). For the bending tests, specimens with 80 mm × 10 mm × 4 mm were tested in a three-point setup with a support length of 64 mm and a speed of 5 mm min^{-1}. Flexural strength was determined with Eq. (2), based on ISO 178:

$$\sigma = \frac{3 \bullet F \bullet L}{2 \bullet b \bullet h^2} \quad (2)$$

where F is the maximum force, L is the span length, b is specimen width, and h is specimen thickness.

The flexural modulus of the specimens in the bending tests is calculated according to (3):

$$E_h = \frac{L^3}{4 \bullet b \bullet h^3} \bullet \frac{\Delta F}{\Delta f} \quad (3)$$

where E_h is the flexural modulus, L is the span length, b is specimen width, h is specimen thickness, and $\frac{\Delta F}{\Delta f}$ is the slope of the force–strain curve of the specimen.

Results and discussion

Physical and mechanical characterization

Appearance of the flame-retarded epoxy resin

The results of the color analysis of the prepared epoxy specimens (according to Table 1) are presented in Table 3. The additive-free reference sample Z0-G0 had an RGB (211, 208, 174) code and a grayscale number of 205.5, and showed a transparent yellowish-brownish character, which allowed the particles dispersed in it to color the matrix. In Table 3, the grayscale column shows that even with 10 mass% ZnO, whitening was significant (with a grayscale value of 245.3), which further increased with increasing ZnO content. With 30 mass% ZnO, the grayscale value was close to the maximum of 255, which indicates complete whiteness. On the other hand, even with 5 mass% EG, the samples showed significant blackening, but completely black with a grayscale value of 0 was not reached, as the EG particles appeared in silvery, grayish shades in the sample in many cases.

We investigated the synergistic effect of ZnO and EG. The samples became whiter as ZnO content was increased. With 5 mass% EG and 10 mass% ZnO, the grayscale value of the samples was 129.9, and with 30 mass% ZnO, it was 177.4. Samples containing 10 mass% EG had a grayscale value of 67.0, but they also became whiter as a result of ZnO.

Table 3 Results of the color analyses and appearance

Sample	RGB code (average)	Grayscale value (average)	Appearance
Z0-G0	(211, 208, 174)	205.5	
Z10-G0	(251, 245, 229)	245.3	
Z20-G0	(252, 247, 236)	247.8	
Z30-G0	(253, 252, 240)	251.5	
Z0-G5	(64, 68, 68)	67.6	
Z10-G5	(121, 132, 140)	129.9	
Z20-G5	(152, 164, 174)	162.2	
Z30-G5	(167, 179, 191)	177.4	
Z0-G10	(64, 68, 67)	67.0	
Z10-G10	(99, 109, 118)	107.3	
Z20-G10	(129, 143, 156)	140.8	
Z30-G10	(144, 159, 172)	156.6	

With 10 mass% ZnO, the grayscale value of the samples was 107.3, and with 30 mass% ZnO, it was 156.6. Samples containing both ZnO and EG have grayscale values between what ZnO or EG would produce alone. More ZnO makes the color whiter, and more EG makes the color darker.

Mechanical properties of the flame-retarded epoxy resin

Figure 1 shows the results of the three-point flexural tests. During the bending tests, the reference specimen had a flexural strength of 88.1 MPa (Fig. 1a). The specimens containing only ZnO (blue bars in Fig. 1a) had a decrease in strength of nearly 10% with 10 mass% ZnO. With 20 mass% ZnO loading, flexural strength was higher, only less by 1% compared to the reference. Therefore, with increasing ZnO content, there is an initial decrease in flexural strength, but it increases with more ZnO, reaching a local maximum, after which flexural strength decreases again. This phenomenon can also be observed for other nano- and micro-sized fillers, such as carbon nanotubes or metal oxides [28, 29]. The particles may not form an efficient network at lower filler contents, but as filler content is increased, mechanical properties improve. More particles are better distributed and can better prevent crack propagation. The movement of the polymer chains is also increasingly inhibited, which increases flexural strength. However, with more ZnO, the system becomes overloaded, and the particles cannot be properly distributed, so local inhomogeneities and aggregates are produced, weakening flexural strength.

The flexural strength of samples containing only EG also decreased (nearly 36% for 5 mass% EG and 45% for 10 mass% EG). This significant reduction was due to the relatively large grain size and the structure of the EG particles, which often formed clusters that could become a defect site in mechanical tests.

Samples with both ZnO and EG showed a strength reduction of 10–39%, which was between the flexural strength reduction of samples loaded with ZnO and EG only. Compared to samples with EG alone, samples with both EG and ZnO had better flexural strength, suggesting that the ZnO particles facilitated the better dispersion of EG. This better dispersion is because the ZnO particles were spherical, whereas the EG particles were flat. During mixing, the differences in the shape of the two particles had a positive effect on the dispersion of both, a phenomenon known in the literature [30].

The flexural modulus of the reference sample was 2.91 GPa. There was an increase in the flexural modulus of elasticity compared to the reference when ZnO or EG was applied alone and also when they were used together (Fig. 1b). For the samples with ZnO only, the variance of the modulus increased with increasing loading, which was due to the higher possibility of aggregates. The modulus and the variance of the measured samples increased with increasing amounts of EG. For samples containing both ZnO and EG, variance behaved differently. The modulus of samples containing 5 mass% or 10 mass% EG also increased with increasing ZnO content. However, as modulus increased,

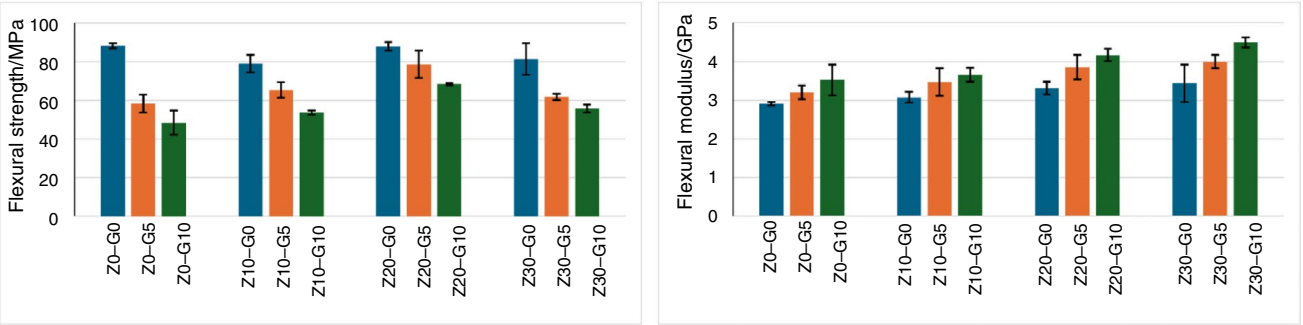

Fig. 1 **a** The flexural strength and **b** the flexural modulus of the flame-retarded epoxy resins

variance decreased. These results also suggest that using ZnO and EG together results in better mixing.

Thermal tests

Thermal stability of the flame-retarded epoxy resin

Table 4 contains the TGA results.

In nitrogen atmosphere, the temperature of 5% mass loss ($T_{-5\%}$) of the reference sample was 278 °C, above which there was rapid mass loss, a typical characteristic of pentaerythritol-based epoxy resins [31]. This sudden mass loss was similar in the behavior of the flame-retardant samples.

For samples containing only ZnO, $T_{-5\%}$ first decreased, then, with increasing ZnO content, $T_{-5\%}$ increased, indicating that ZnO improved the thermal stability of the matrix. $T_{-5\%}$ decreased when only EG was added because EG starts to exhibit its effects around 200–250 °C. For the mixed samples, $T_{-5\%}$ increased with increasing ZnO content. The temperature at 50% mass loss ($T_{-50\%}$) increased in all cases compared to the reference value (319 °C). Since there is no mass loss of ZnO up to 600 °C, $T_{-50\%}$ increased with increasing amounts of ZnO. With increasing EG content, $T_{-50\%}$ decreased. The volume of EG increases, and its mass decreases (it decomposes and gases are released) as temperature increases, and by the time the temperature reached 319 °C, all the decomposition (and mass loss) had taken place. In the case of mixed samples, the increase in $T_{-50\%}$ was more significant than the increase with ZnO or EG only, suggesting a synergism. The literature suggests that EG and metal oxides interact positively to improve thermal properties [32], which was the case for EG and ZnO.

The maximum mass loss rate (dTG_{max}) of the reference sample was 2.93% $°C^{-1}$. All samples had more than half the dTG_{max} values compared to a reference sample. The explanation for this reduction is that the nanoparticles caused a more controlled, slower degradation in the samples. The lowest dTG_{max} was obtained for the samples containing 5 mass% EG and 20 mass% ZnO. The temperature for the maximum mass loss rate (T_{dTGmax}) was lower than that of the reference (280 °C) in all cases except for Z0-G10. In this case, the decrease (12 °C) can be explained by the mass loss due to the volume expansion of EG. Z0-G10 had a lower dTG_{max} value than the reference but had more controlled decomposition.

The residual mass of the reference sample was 8.9% at 600 °C, a value that increased proportionally with the amount of flame retardants in all cases. There was always more residual mass in the system than the mass of the flame retardants, which is consistent with the idea that the flame-retardant particles could contribute to the formation of the char layer by interacting with the residual epoxy resin material.

We also performed TGA measurements in a thermo-oxidative atmosphere (in air atmosphere) to see how the material properties change in an oxidizing environment. In the case of $T_{-5\%}$ values, the decomposition started earlier in the air atmosphere than in the nitrogen atmosphere for almost all samples. The reason for this difference is that in an air atmosphere, oxidation also contributes to the decomposition of the samples, which starts at lower temperatures, while in

Table 4 TGA results depending on the amount of ZnO and EG

Sample	In nitrogen atmosphere					In air atmosphere				
	$T_{-5\%}$/°C	$T_{-50\%}$/°C	dTG_{max}/ % $°C^{-1}$	T_{dTGmax}/°C	Residue at 600 °C/%	$T_{-5\%}$/°C	$T_{-50\%}$/°C	dTG_{max}/% $°C^{-1}$	T_{dTGmax}/°C	Residue at 600 °C/%
Z0-G0	278	319	2.93	280	8.9	256	324	1.36	287	8.9
Z10-G0	274	338	1.01	295	23.2	260	356	0.98	303	15.6
Z20-G0	282	419	1.24	306	32.9	271	468	1.26	308	16.1
Z30-G0	290	530	1.29	309	44.6	281	501	1.26	309	26.0
Z0-G5	271	341	0.97	288	17.4	266	324	1.26	286	5.6
Z10-G5	270	351	0.87	302	28.7	264	320	2.90	268	10.5
Z20-G5	275	330	1.10	308	44.0	268	471	1.10	308	20.2
Z30-G5	282	-	0.97	311	51.3	270	510	1.10	311	32.6
Z0-G10	252	334	1.24	268	21.4	258	342	0.99	297	12.6
Z10-G10	264	351	1.01	285	29.7	232	439	0.85	308	15.5
Z20-G10	272	498	0.95	310	41.9	274	495	1.01	311	25.0
Z30-G10	274	-	0.80	311	51.1	270	507	1.17	313	34.9

($T_{-5\%}$: temperature at 5% mass loss, $T_{-50\%}$: temperature at 50% mass loss, dTG_{max}: maximum mass loss rate, T_{dTGmax}: the temperature belonging to the maximum mass loss rate)

a nitrogen atmosphere, only thermal decomposition occurs. The $T_{-5\%}$ value of the reference Z0-G0 sample in air was 256 °C, which increased by the influence of flame retardants, except for the Z10-G10 sample. The $T_{-50\%}$ value of the reference was 324 °C, which was 5 °C higher than the same value in nitrogen atmosphere. Due to the effect of flame retardants, the $T_{-50\%}$ increased compared to the reference, with the exception of two samples (Z0-G5 and Z10-G5). The $T_{-50\%}$ of samples containing 30 mass% ZnO was above 500 °C in all cases. The dTG_{max} value for the reference was 1.36% $°C^{-1}$, which decreased due to the effect of the flame retardants. The temperature corresponding to dTG_{max} increased compared to the reference, except for samples Z0-G5 and Z10-G5. The mass remaining at 600 °C was lower in all cases than the masses measured in a nitrogen atmosphere. This can be explained by the fact that in an air atmosphere, the solid residues can oxidize further under the influence of the oxidative atmosphere, while in an inert atmosphere they remain unchanged.

Flame retardancy of the flame-retarded epoxy resin

The samples were tested for flammability with UL-94, LOI, and MLC tests. Table 5 contains the results of the UL-94 and LOI tests, and Table 6 contains those of MLC.

Although all UL-94 samples were HB-rated, the processes that occurred were different for different additive ratios. The burning rate of the reference sample was 26.6 mm min^{-1}, and all samples burned entirely. There were large amounts of sooty smoke and flying ash particles during burning.

For samples containing only ZnO, the ZnO formed a protective layer on the burning surface, which held the specimen and the burn residue together [33]. A reduction in the burning rate was only achieved with 30 mass% ZnO because metal oxides only produce good flame retardancy in polymer matrices in higher amounts [34]. The flame was sooty, but there was not much flying ash. With 30 mass% ZnO, there was a smaller sooty flame with intense foaming. The ZnO caused a twisting (Fig. 2a) charred residue with a layered structure. In a few cases with 30 mass% ZnO, combustion was extinguished before the second signal, because the twisted charred residues fell off. Compared to the reference, the addition of 10 mass% ZnO reduced the burning time, but as the amount of ZnO increased, the burning time also tended to increase.

In total, 5 mass% EG reduced the burning rate and increased the burning time. Samples had typical "worm-like" formations when EG was added (Fig. 2b). Consequently, the residue of the samples containing only EG quickly disintegrated, often producing flying ash. However, the resulting charred residue had a stable structure when 5 mass% EG and ZnO were used together. As a result, the

Table 5 The UL-94 and LOI results of the flame-retarded epoxy resins

Sample	Horizontal test					Vertical test			UL-94 ranking	LOI/volume%
	Completed the horizontal test?	Burning time/s	Burnt through?	Average burned length/mm	Burning rate/mm min^{-1}	Cotton wool was ignited?	Did it burn up completely?	Burning time/s		
Z0-G0	No	170 ± 17	yes	75	26.6 ± 2.9	–	–	–	HB/27	22
Z10-G0	No	151 ± 5	yes	75	29.8 ± 1.0	–	–	–	HB/30	24
Z20-G0	No	165 ± 9	yes	75	27.2 ± 1.6	–	–	–	HB/27	25
Z30-G0	No	176 ± 2	yes	75	24.6 ± 1.6	–	–	–	HB/24	27
Z0-G5	No	197 ± 6	yes	75	22.9 ± 0.7	–	–	–	HB/23	24
Z10-G5	No	321 ± 31	yes	75	14.1 ± 1.3	–	–	–	HB/14	27
Z20-G5	No	92 ± 14	no	19	12.4 ± 2.1	–	–	–	HB/12	25
Z30-G5	No	68 ± 25	no	13	11.6 ± 0.9	–	–	–	HB/12	25
Z0-G10	No	389 ± 12	yes	75	11.6 ± 0.4	–	–	–	HB/12	24
Z10-G10	Yes	–	–	–	–	no	yes	40 ± 7	HB	25
Z20-G10	Yes	–	–	–	–	no	yes	43 ± 10	HB	25
Z30-G10	Yes	–	–	–	–	no	yes	57 ± 11	HB	27

(Average standard deviation of the LOI: ± 1 volume%)

Table 6 MLC results of the reference and the flame-retarded epoxy resins

Sample	TTI/s	pHRR/kW m^{-2}	t_{pHRR} /s	THR/MJ m^{-2}	Residue/%	MARHE/ kW m^{-2} s^{-1}	EHC/MJ kg^{-1}
Z0-G0	122	1086	192	86	3	304	598
Z10-G0	91	912	152	76	25	304	55
Z20-G0	112	829	167	55	33	222	30
Z30-G0	148	1030	188	54	40	196	22
Z0-G5	115	994	202	70	8	236	172
Z10-G5	132	814	201	57	32	197	32
Z20-G5	141	765	192	53	39	187	24
Z30-G5	138	716	188	48	46	175	17
Z0-G10	170	776	241	67	13	188	105
Z10-G10	157	865	205	54	35	185	26
Z20-G10	164	870	208	54	41	176	20
Z30-G10	135	740	196	53	47	186	16

(TTI: time to ignition, pHRR: peak heat release rate, t_{pHRR}: time to peak heat release rate, THR: total heat release, MARHE: maximum average rate of heat emission, EHC: effective heat of combustion)

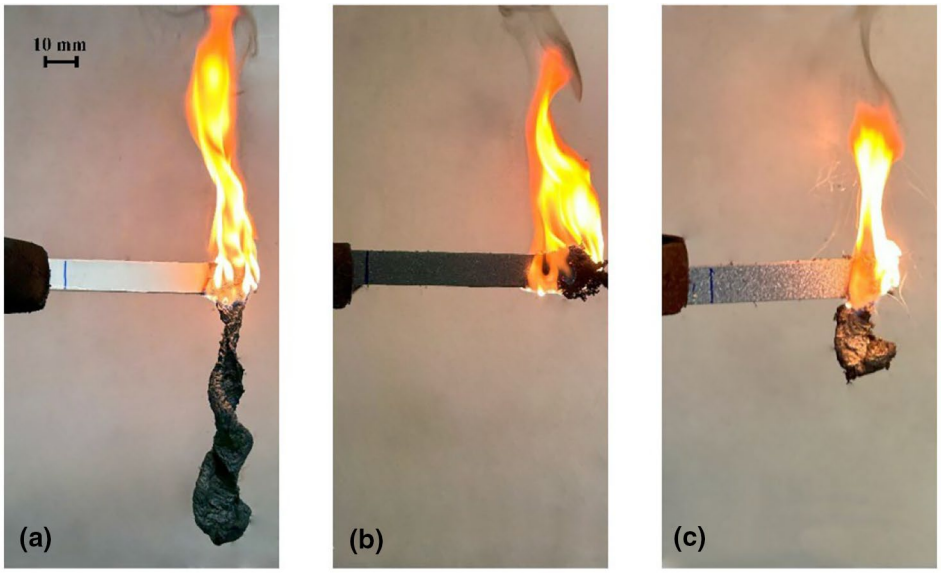

Fig. 2 UL-94 test: **a** the burning of a samples containing only ZnO, **b** the burning of a sample containing only EG, and **c** the burning of a sample containing both flame retardants

burning rates were significantly reduced with the flame-retardant additives compared to the reference. The Z30-G5 sample had a reduction in burning rate of more than 50%. With 5 mass% EG and 20 mass% or 30 mass% ZnO, the sample was extinguished before the second signal, indicating that a further increase in EG could further improve flame resistance. The burned length of the Z20-G5 sample was 19 mm after the first mark, while that of the Z30-G5 sample was 13 mm. Thus, the shorter burning distance also reduced the burning time. The burn residue was stable for samples with both EG and ZnO (Fig. 2c).

With 10 mass% EG, even the ZnO-free sample had a significantly reduced burning rate (11.6 mm min^{-1}) and increased the burning time (389 s). In the case of samples containing ZnO and 10 mass% EG, the flame did not reach the first mark in the horizontal test, but in the vertical test, the samples burned up to the holding clamp. Since V ratings do not allow full burning, all samples received an HB rating without burning rate. During the vertical test, the total burning time after the first and second ignitions increased with increasing ZnO content. Twisted char residue appeared, but the cotton wool did not ignite when it dripped down.

The oxygen index of the reference sample was 22 volume%, which was increased in all cases by the flame retardants. The oxygen index increased with increasing ZnO for samples containing only ZnO. There was intense foaming, also present in UL-94, so LOI values increased. Samples containing only EG also had increased LOI values (to 24 volume%). In all cases, adding ZnO to samples containing EG increased the oxygen index but not proportionally to

the amount of ZnO. There was a sharp limit for almost all samples, as in most cases, the samples were extinguished after only a few seconds of burning at a value below the oxygen index.

The complex burning properties of the samples were investigated by mass loss type cone calorimetry. Figure 3 shows the MLC curves, and Table 6 shows the results.

The time to ignition (TTI) of the reference sample was 122 s. With the addition of 10 mass% ZnO, the TTI decreased by 31 s. With an increase in the amount of ZnO, the TTI increased for samples containing only ZnO. The most significant increase in TTI was obtained for the sample containing 10 mass% EG, where an increase of 48 s was required to ignite the sample compared to the reference. In all cases, samples containing both EG and ZnO increased the TTI.

The peak heat release rate (pHRR) of the reference sample was 1086 kW m^{-2}, which decreased for all flame-retarded samples. For the samples containing only ZnO, the pHRR decreased by 5–24%, but these values may have been minimally distorted due to the uncontrolled foaming during burning. The foam may have touched the heating element of the testing device, which may have influenced the measured values. The sample Z30-G5 showed the most significant decrease in pHRR (34.1%) compared to the reference. All samples containing 10 mass% EG showed a reduction in pHRR of at least 19% compared to the reference.

The reference sample reached its pHRR after 192 s (t_{pHRR}), which was reduced by ZnO, so it reached its peak heat release rate sooner. This reduction is due to the residue from burning containing ZnO, which increased the heat release. In the case of solid-phase flame retardants, heat release is usually characterized by a massive increase until the formation of a char layer, after which heat release starts to decrease [35]. EG increased t_{pHRR} compared to the reference. The time to peak heat release rate was the shortest for the pure epoxy, longer with ZnO, even longer with both flame retardants, and it was the longest with EG only.

In all cases, total heat release (THR) decreased compared to the reference value of 86 MJ m^{-2}. THR decreased with increasing amounts of ZnO or EG when the flame retardants were used alone. In samples with both flame retardants, ZnO reduced the THR of the EG samples in all cases, indicating that they interacted.

As expected, the residual mass of the reference sample after combustion was minimal (3%). In contrast, the flame retardants increased residual mass. ZnO increased the residual mass to a high percentage in all cases. EG alone increased the residual mass to a lower percentage than ZnO.

To evaluate the mechanism of the flame retardants, we also investigated the maximum average rate of heat emission (MARHE) and the effective heat of combustion (EHC). The MAHRE was 304 kW m^{-2} s^{-1} for the reference, and for the sample which contained only 10 mass% ZnO. However, apart from these two samples, MARHE decreased significantly due to the effect of the flame retardants. The best MARHE was that of the Z30-G5 sample (175 kW m^{-2} s^{-1}). The significant reduction in MARHE indicates that flame retardants effectively limit the amount of heat released during combustion due to the protective layer.

The EHC of the reference sample was 598 MJ kg^{-1}. In all cases, the flame retardants significantly reduced this value, and sample Z30-G10 had the lowest EHC (16 MJ kg^{-1}). EHC decreased by more than 90% for all samples containing ZnO only, while it was reduced by more than 70% for samples containing only EG. This significant decrease in EHC suggests that the flame retardants prevent complete burning, typically by promoting the formation of nonflammable residues (for example, carbonaceous char) or by releasing nonflammable gases (for example, water vapor, CO_2, or ammonia) [36, 37]. The fact that both MAHRE and EHC were significantly reduced when the flame retardants were used together indicates that the flame retardants work together primarily in the condensed phase. When used together, they strongly promote char formation during combustion and form a thermal barrier, which inhibits heat transfer.

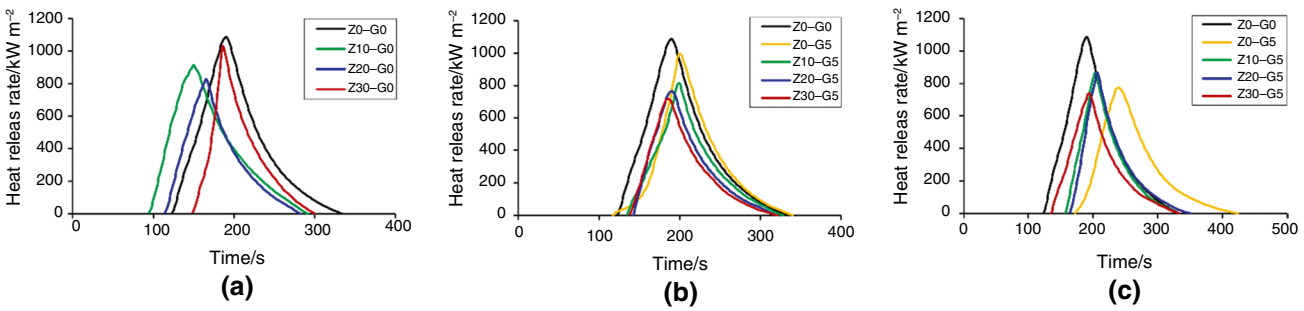

Fig. 3 MLC curves of flame-retarded epoxy resins, **a** the curves of the sample group containing no EG, **b** the curves of the sample group containing 5 mass% EG, and **c** the curves of the sample group containing 10 mass% EG

Gases from combustion

Figure 4 shows the results of the LP-FTIR tests. The tests were performed for all sample types (pure epoxy, epoxy with only ZnO, epoxy with only EG, and epoxy with both ZnO and EG).

Figure 4 shows an intense and wide peak in the reference sample between 3550 and 3100 cm^{-1}, which can be attributed to the N–H stretching vibrations from the cross-linking agent (modified cycloaliphatic amine), and a peak between 3200 and 2800 cm^{-1} can be attributed to the C-H stretching vibrations. According to the literature [38], if zigzag peaks appear between 4000 and 3500 cm^{-1} and 2000 and 1500 cm^{-1}, it may be because of the water vapor generated. Furthermore, peaks in the range 2000–1500 cm^{-1} may also be attributed to water vapor, but C = O stretching and N–H bending oscillations may also appear in this range. The CO_2 characteristic peaks are between 2400 and 2300 cm^{-1}, while the CO characteristic peaks are between 2200 and 2080 cm^{-1}. In the 1300–1000 cm^{-1} range, C–O–C and C-N stretching appeared, while C-H vibrations appeared between 1500 and 1400 cm^{-1}.

With 10 mass% EG, the N–H, C-H, C–O–C, and C-N vibrations from the resin almost disappeared, and the intensity of the CO_2 and CO peaks was significantly reduced. This reduction suggests that the expandable graphite acts mainly in the condensed phase, forms a charred protective layer on the surface of the sample, and does not generate large amounts of gas-phase volatile chemicals. This statement is in agreement with the literature [39]. Furthermore, there are also water vapor peaks in the Z0-G10 sample.

For the sample containing only 30 mass% ZnO, the intensity of the peaks from the decomposition of the resin is significantly reduced, but the water vapor-related regions (3550–3100 cm^{-1}) still exist. Furthermore, CO_2 emission appeared at a higher intensity peak (2400–2300 cm^{-1}) compared to the reference, and CO absorption peaks were also higher. New peaks appeared in the range 700–400 cm^{-1}, which can be attributed to Zn–O vibrations [40].

The spectra of the sample containing both ZnO and EG were similar to those of the sample containing only ZnO, but the intensity of the CO_2 and CO peaks increased further. In addition, the Zn–O vibrational peaks were also higher in intensity due to the effect of the mixed composition, suggesting that the expandable graphite may affect the structure or decomposition mechanism of ZnO.

Analysis of the residual structure

The structure and composition of the residues were studied by optical microscopy and scanning electron microscopy. Figure 5 shows optical microscope images of the surface of the combustion residues.

Figure 5a shows the pure sample. The surface image shows that residues had a consistent structure. The figure shows hollows, which are the exit points for the gases escaping during burning. Figure 5b shows the surface of a sample containing only ZnO. The ZnO particles are visible on the surface of the sample, and they are embedded in the residue. [33]. The structure of the residue from the sample containing only ZnO did not disintegrate due to the presence of ZnO, forming a 'puff pastry-like' shape. While it could hold

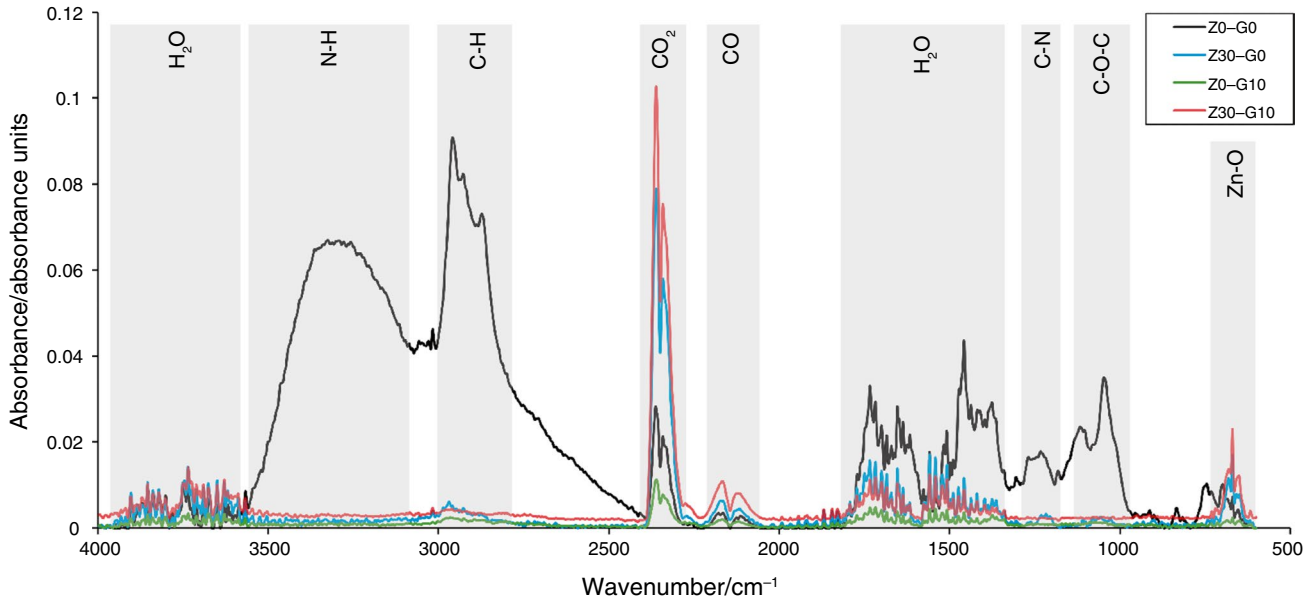

Fig. 4 LP-FTIR results and the gaseous chemicals produced

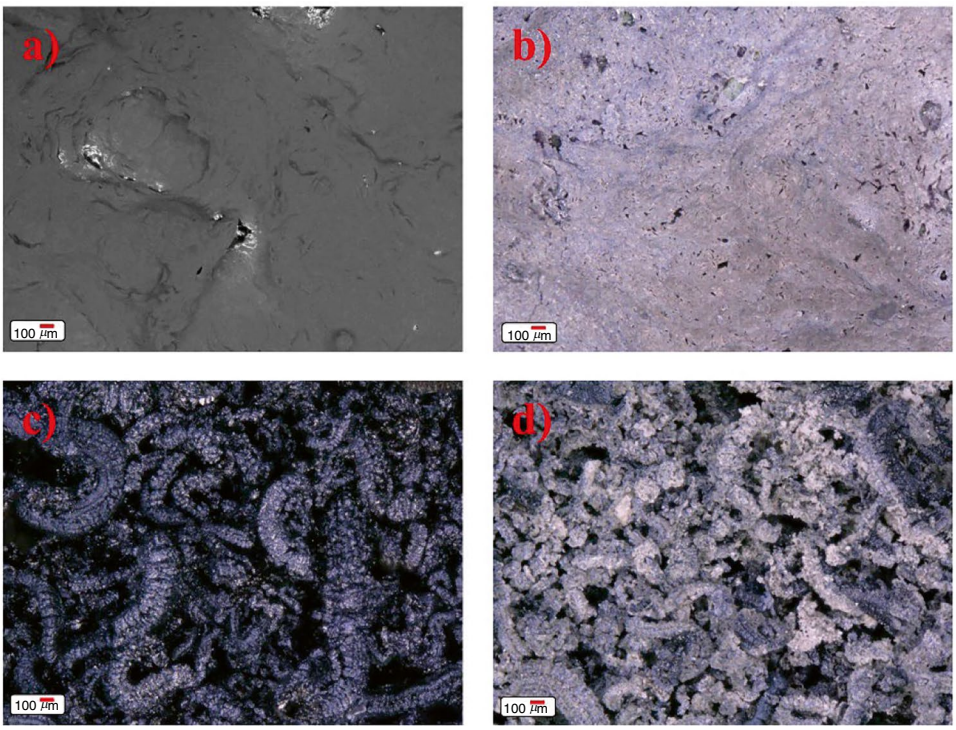

Fig. 5 Surface structure of char residues: **a** pure epoxy, **b** sample containing only ZnO, **c** sample containing only EG, **d** sample containing both ZnO and EG

together on its own, it was easily fragmented under minimal mechanical load. The surface of the residue (Fig. 5b) is visibly whitened. Figure 5c shows the structure of a sample containing only EG. The figure clearly shows the separate "worm-like" formations produced by EG. Thus, there was no significant cohesive force in the structure. Figure 5d shows the structure of the residue of the sample containing ZnO and EG. The figure clearly shows the "worm-like" formations created by EG, and the ZnO particles that whitened the surface of the residue. Furthermore, the resulting structure of the residue had a structurally more stable surface, which was less susceptible to mechanical damage than samples containing only EG.

Figure 6a shows the structure of combustion residues of the pure epoxy matrix. What remains is amorphous char with minimal residual mass. Figure 6b is an SEM image of the structure, which is solid char. SEM–EDS showed that 80.6–82.2 mass% of the residual material was carbon and 17.8–19.4 mass% was oxygen.

Figure 7a shows the structure of the residue of the Z30-G0 sample (with only ZnO) after burning. The samples containing only ZnO were characterized by the formation of a "puff pastry-like" structure during burning. The thick layers remained intact during burning due to the effect of ZnO. Still, the gases released from the epoxy resin during combustion expanded the epoxy, giving it a characteristic structure. Figure 7b shows the upper parts of a sample containing only ZnO, which burned intensely. The intense gas formation produced a membranous structure with bubbles. Figure 7c

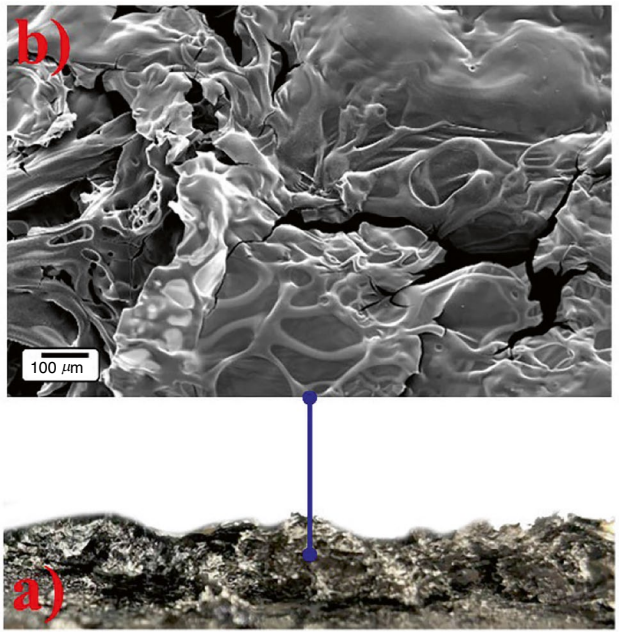

Fig. 6 Combustion residue **a** of pure epoxy (inside, side view), **b** of pure epoxy

shows the side of the samples containing only ZnO. A more stable, coherent layer of material formed, in which there were holes of a few nm, which allowed the gases to escape but produced a thicker char layer. The sample residue consisted of 14.6–23.7 mass% carbon, 7.1–17.5 mass% oxygen,

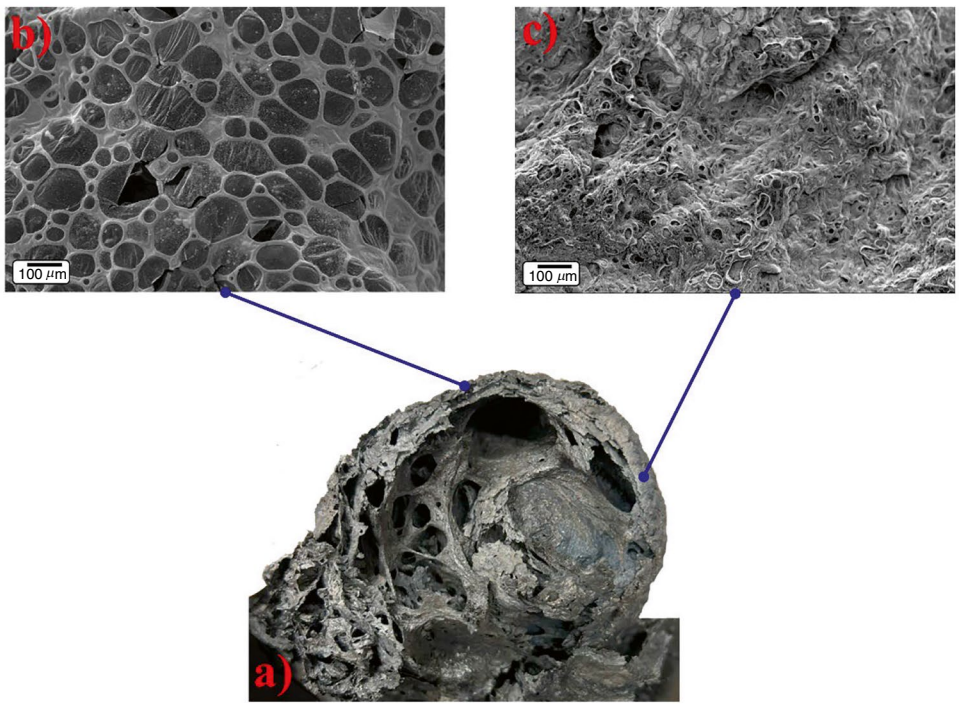

Fig. 7 Combustion residue: **a** side view of the inside of the residue of the sample with ZnO, **b** SEM image of the residue of the sample with only ZnO in the more intensively burned part, **c** SEM image of the residue of the sample containing only ZnO in the less intensively burnt part

6.1–6.9 mass% chlorine, and 60.9–63.2 mass% zinc. The top of the sample contained 32.7–35.5 mass% carbon, 7.5–11.7 mass% oxygen, 13.5–14.3 mass% chlorine, and 39.3–45.5 mass% zinc. The results showed that chlorine was also present in the epoxy system, which was bound by the ZnO and thus became detectable. Epoxy resins may contain hydrolyzable chlorine, which is retained from epichlorohydrin during the epoxy synthesis. It is released from the epoxy system as hydrogen chloride (HCl) during combustion, which is detectable [41]. ZnO can bind chlorine [42], in this case by binding it to the structure of the residue. We found that there was Cl enrichment in the upper layers because more of it was released, but ZnO absorbed it.

Figure 8a shows the typical combustion residue of samples containing only EG. The residue consisted of "worm-like" forms from EG, produced by heat. The "worm-like" formations were distributed evenly throughout the residue. The protective layer fell apart very easily upon external impact, as it did not have cohesive force, as reported in the literature [39]. Figure 8b shows the "worm-like" structure. The residual sample consisted of 91.1–91.8 mass% carbon and 8.2–8.9 mass% oxygen.

Figure 9a shows the residual structure of samples containing both ZnO and EG particles. The residue shows the characteristics of the residue structures of both flame retardants, and it was stable and more difficult to break. Figure 9b shows the inside of the sample, where the "worm-like" structures are a little further apart. Figure 9c shows the top of the sample which was richer in ZnO. Figure 9d shows the side of the sample, which was apparently more stable, where the

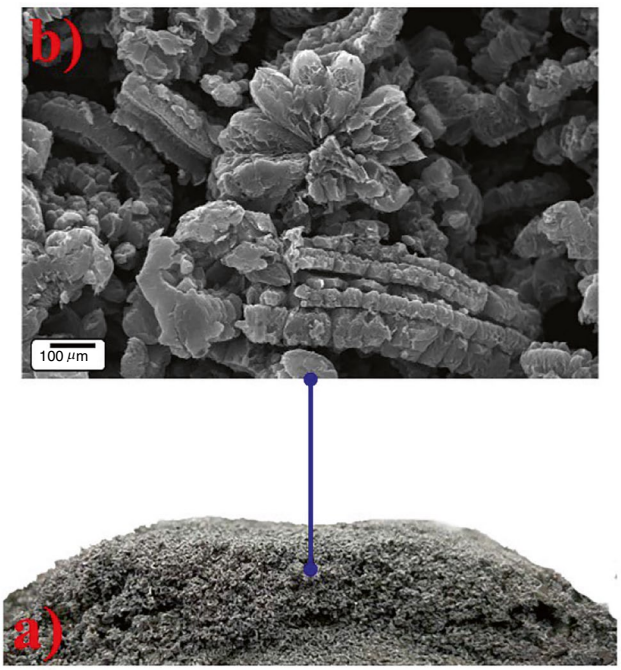

Fig. 8 Combustion residue **a** side view of the inside of the residue of the sample with only EG, **b** SEM image of the residue of the sample with only EG

"worm-like" structures were less discernible. SEM–EDS shows that this sample was able to bind Cl under the influence of ZnO. The interior of the sample contained 3.4–9.0 mass% carbon, 10.1–11.1 mass% oxygen, 21.5–25.3 mass%

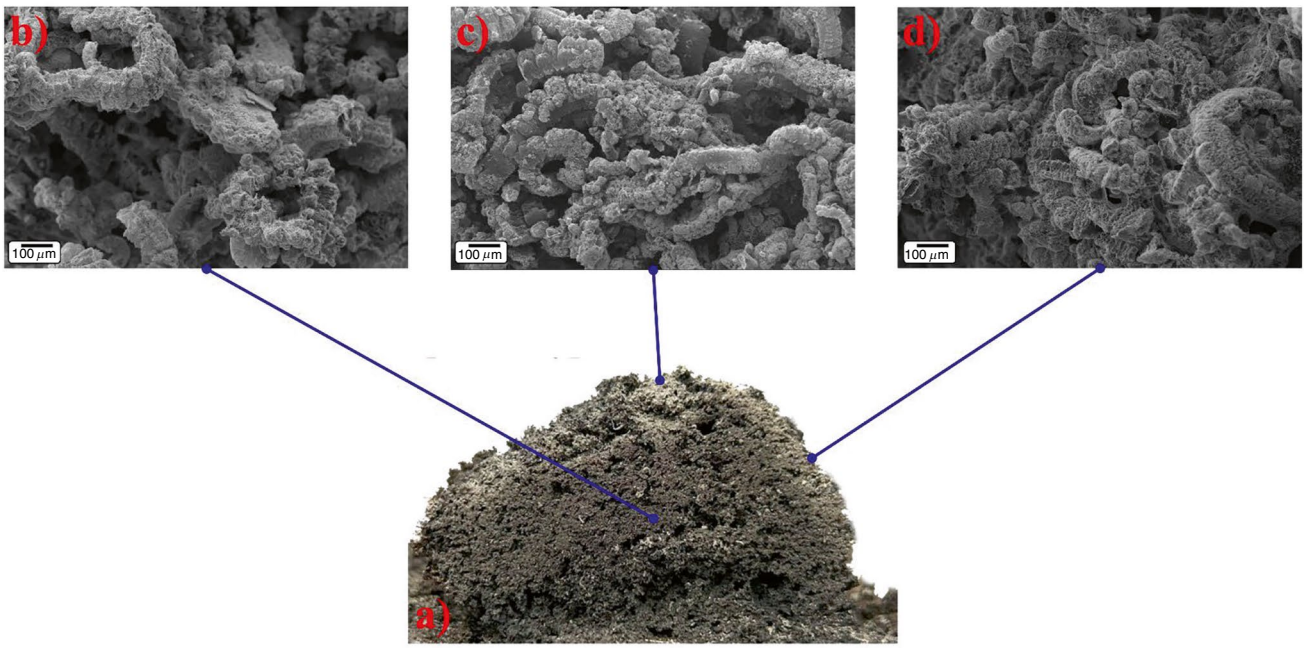

Fig. 9 Combustion residue **a** side view of the inside of the residue containing ZnO and EG, **b** SEM image of the sample containing ZnO and EG on the inside, **c** SEM image of the sample containing ZnO and EG on the top, **d** SEM image of the side of the sample containing ZnO and EG

chlorine, and 55.7–64.1 mass% zinc. The side of the sample consisted of 10.4–42.8 mass% carbon, 2.86–8.7 mass% oxygen, 11.1–15.5 mass% chlorine, and 37.5–71.24 mass% zinc. The top of the sample was 13.6–27.6 mass% carbon, 7.0–9.9 mass% oxygen, 4.2–5.3 mass% chlorine, and 57.23–75.2 mass% zinc. Less chlorine was present at the top of the sample. On the side of the sample, the zinc was able to bind more chlorine. However, the inside of the sample contained a significant amount of chlorine, as the outer protective layer trapped the chlorine in the sample, allowing it to remain in the burn residue and react with the ZnO.

Figure 10 shows the burn residue of all the sample types, with their sizes compared to each other. Figure 10a shows the combustion residue without flame retardants. Figure 10b shows the "puffy pastry-like" structure typical of samples containing only zinc oxide. The thick layers kept the layers together due to the ZnO, but the gases released from the epoxy resin during burning expanded the internal structure, forming a unique structure. Figure 10c shows the typical combustion residue of samples containing only EG. The residue consisted of "worm-like" structures that formed from the EG due to heat, but there was no significant cohesive force between them, so the structure easily disintegrated. Figure 10d shows the burn residue structure of samples containing both ZnO and EG. This time, the structure was similar to the residue structures of both flame retardants. The structure had the "worm-like" formations of EG, but these were better held together by the charred particles together with ZnO, and the hollow "puff pastry-like" structure characteristic of ZnO was not filled with air but with the "worm-like" structures created by EG, forming a more stable structure.

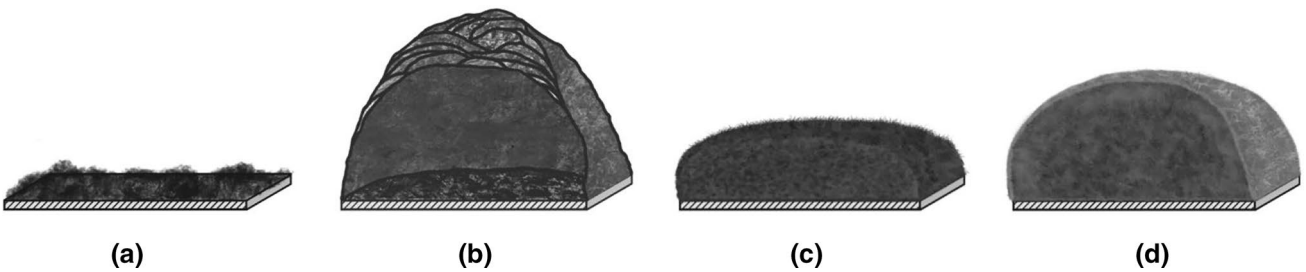

Fig. 10 Image of the internal structure of burn residues, **a** pure epoxy, **b** samples containing only ZnO, **c** samples containing only EG, **d** samples containing both ZnO and EG

Another positive aspect was that the samples with embedded ZnO had chlorine-binding capacity.

Conclusions

In this study, the behavior of epoxy resin was investigated when ZnO and EG were added to it. The coloring effect of these flame-retardant additives in generally transparent epoxy resins was analyzed. Zinc oxide can color composite products light gray, almost white if required, while expandable graphite can make the color of the product a darker gray, in addition to their flame-retardant effect. The two additives can modify the color of the base resin in the grayscale range of 67–255, depending on the ratio of ZnO to EG. We found that the flexural strength of the flame retardant-loaded samples was reduced due to the shape of the dispersed filler particles. However, their flexural modulus of elasticity was significantly increased, by up to 54%, compared to pure epoxy resin, as the embedded flame retardants reduced the mobility of the molecular chains, and thus stiffened the matrix. By combining the two flame retardants, we produced a completely condensed-phase intumescent flame-retardant system with lower heat release during combustion. The effective heat of combustion (EHC) of samples containing both ZnO and EG was reduced by up to 97%, while their maximum average rate of heat emission (MAHRE) was reduced by nearly 40% compared to pure epoxy. Zinc oxide causes significant foaming, creating a layered, "puff pastry-like" structure, as it can hold the burned residue together and stabilize it. The residue with the 'worm-like' structure, typical of expandable graphite (EG), can be made more stable by zinc oxide, as the solid metal oxide particles interact with the combustion residue, helping to hold it together. This results in a large, stable foam structure that enhances the amount and improves the properties of the intumescent foam. The combination of ZnO and EG significantly reduces the typical combustion gases evolved from epoxy resins, such as those containing C-H and N–H bonds. ZnO in epoxy resins can successfully bind the chlorine left over from the production of the epoxy resin while it is released from the polymer material and can, therefore, make the epoxy matrix less harmful when it burns. As a result, ZnO may be useful as a flame retardant in products where chlorine is present.

Acknowledgements The research reported in this paper was supported by the National Research, Development, and Innovation Office (NRDI, Hungary) through grants OTKA K 146236, OTKA K 138472, and OTKA K 142517. Project no. TKP-6-6/PALY-2021 has been implemented with the support provided by the Ministry of Culture and Innovation of Hungary from the National Research, Development and Innovation Fund, financed under the TKP2021-NVA funding scheme. The project 2022-2.1.1-NL-2022-00012 has been implemented with the support provided by the Ministry of Culture and Innovation of Hungary from the National Research, Development and Innovation Fund, financed under the 2022-2.1.1-NL Creation of National Laboratories, Complex Development funding scheme. Péter Csvila expresses appreciation for the support of the Doctoral Excellence Fellowship Programme (DCEP) funded by the National Research Development and Innovation Fund of the Ministry of Culture and Innovation and the Budapest University of Technology and Economics, under a grant agreement with the National Research, Development and Innovation Office.

Funding Open access funding provided by Budapest University of Technology and Economics. Nemzeti Kutatási,Fejlesztési és Innovációs Alap,OTKA K 146236,OTKA K 138472,OTKA K 142517,TKP-6-6/PALY-2021,TKP2021-NVA,2022-2.1.1-NL-2022-00012,Doctoral Excellence Fellowship Programme (DCEP),Péter Csvila

Data availability All data generated or analyzed during this study are included in the present article.

Open Access This article is licensed under a Creative Commons Attribution 4.0 International License, which permits use, sharing, adaptation, distribution and reproduction in any medium or format, as long as you give appropriate credit to the original author(s) and the source, provide a link to the Creative Commons licence, and indicate if changes were made. The images or other third party material in this article are included in the article's Creative Commons licence, unless indicated otherwise in a credit line to the material. If material is not included in the article's Creative Commons licence and your intended use is not permitted by statutory regulation or exceeds the permitted use, you will need to obtain permission directly from the copyright holder. To view a copy of this licence, visit http://creativecommons.org/licenses/by/4.0/.

References

1. Marton GZ, Szebényi G. Influencing the damage process and failure behaviour of polymer composites – a short review. Express Polym Lett. 2025. https://doi.org/10.3144/expresspolymlett.2025.11.
2. Wang H, Wang Y, Yu C, Xing X, Lin P, Liu J, et al. Synthesis of an environmentally friendly P–N synergistic flame retardant and its effect on the properties of epoxy resin. Adv Ind Eng Polym Res. 2025. https://doi.org/10.1016/j.aiepr.2024.12.001.
3. Huang Y, Yang W, Zhao Y, Miao Y, Wang J, Lu Y, et al. Hydrangea inspired hierarchical polyphosphazenes/molybdenum diselenide flame retardant as efficient enhancer for epoxy resin. Appl Surf Sci. 2025. https://doi.org/10.1016/j.apsusc.2024.162003.
4. Bifulco A, Varganici C, Rosu L, Mustata F, Rosu D, Gaan S. Recent advances in flame retardant epoxy systems containing non-reactive DOPO based phosphorus additives. Polym Degrad Stab. 2022. https://doi.org/10.1016/j.polymdegradstab.2022.109962.
5. Toldy A, Szolnoki B, Marosi Gy. Flame retardancy of fibre-reinforced epoxy resin composites for aerospace applications. Polym Degrad Stab. 2011. https://doi.org/10.1016/j.polymdegradstab.2010.03.021.
6. Gao M, Wu W, Yan Y. Thermal degradation and flame retardancy of epoxy resins containing intumescent flame retardant. J Therm Anal Calorim. 2009. https://doi.org/10.1007/s10973-008-9766-8.
7. Jauregui Rozo M, Sunder S, Ruckdäschel H, Schartel B. Char, gas, and action: transfer of the flame-retardant modes of action in epoxy resins and their fiber-reinforced composites. Polym Test. 2024. https://doi.org/10.1016/j.polymertesting.2024.108610.
8. Yang S, Wang J, Huo S, Cheng L, Wang M. Preparation and flame retardancy of an intumescent flame-retardant epoxy resin system constructed by multiple flame-retardant compositions containing

phosphorus and nitrogen heterocycle. Polym Degrad Stab. 2015. https://doi.org/10.1016/j.polymdegradstab.2015.05.019.
9. Zhai X, Ma Q, Lu J, Jin Y, Zhang R, Luo F. Enhanced thermal stability and flame retardancy of PLA through intumescent flame retardant with B-modified ZSM-5 as a synergistic agent. Express Polym Lett. 2024. https://doi.org/10.3144/expresspolymlett.2024.23.
10. Mohd Sabee MMS, Itam Z, Beddu S, Zahari NM, Mohd Kamal NL, Mohamad D, et al. Flame retardant coatings: additives, binders, and fillers. Polymers. 2022. https://doi.org/10.3390/polym14142911.
11. Zhan Z, Shi J, Zhang Y, Zhang Y, Zhang B, Liu W. The study on flame retardancy synergetic mechanism of magnesium oxide for PA66/AlPi composite. Mater Res Express. 2019. https://doi.org/10.1088/2053-1591/ab4737.
12. Zhang T, Wang C, Bo R, Han Z. The effect of metal oxide and polycarbosilane on flame retardancy and combustion behavior of Eva/MH composites. J Appl Polym Sci. 2025. https://doi.org/10.1002/app.57043.
13. Cheng C, Shuqian S, Mingmei S, Zhengwen W, Xingrong Z, Linsheng T. Synergistic flame retardancy of ZnO with piperazine pyrophosphate/melamine polyphosphate in PP. Polym Test. 2023. https://doi.org/10.1016/j.polymertesting.2022.107878.
14. Liu J, Wang R, Liang D, Zhang S, Feng J, Xu M, et al. Highly efficient polyethylene composites with flame-retardant, smoke and toxicity suppression properties by incorporating urchin-like ZnO@C-N and intumescent flame retardant. Polym Degrad Stab. 2025. https://doi.org/10.1016/j.polymdegradstab.2025.111190.
15. Scionti G, Piperopoulos E, Atria M, Calabrese L, Proverbio E. Effect of magnesium hydroxide and aluminum hydroxide as thermal barriers on the flame-retardant behavior of acrylic-based coating. Coatings. 2023. https://doi.org/10.3390/coatings13091517.
16. Lee J, Park JH, Shim SB, Lee JE. Mechanical properties of polypropylene-based flame retardant composites by surface modification of flame retardants. Polymers. 2022. https://doi.org/10.3390/polym14173524.
17. Jiao L-L, Zhao P-C, Liu Z-Q, Wu Q-S, Yan D-Q, Li Y-L, et al. Preparation of magnesium hydroxide flame retardant from hydromagnesite and enhance the flame retardant performance of EVA. Polymers. 2022. https://doi.org/10.3390/polym14081567.
18. Taib MNAM, Khairuddin NFM, Saleh TA. Functionalized carbon nanotubes: synthesis, properties, and application in polymer for flame retardancy—a review. J Therm Anal Calorim. 2025. https://doi.org/10.1007/s10973-025-14016-y.
19. Zhou S-J, Xiong S-J, Yu S, Yuan T-Q. Enhanced flame retardancy and electrical conductivity in nacre-inspired PBAT/montmorillonite/lignin ternary biodegradable composites reinforced with well-dispersed carbon nanotubes. Compos Part B Eng. 2025. https://doi.org/10.1016/j.compositesb.2025.112214.
20. Tomiak F, Schoeffel A, Rathberger K, Drummer D. Expandable graphite, aluminum diethylphospinate and melamine polyphosphate as flame retarding system in glass fiber-reinforced PA6. Polymers. 2022. https://doi.org/10.3390/polym14061263.
21. Modesti M, Lorenzetti A. Halogen-free flame retardants for polymeric foams. Polym Degrad Stab. 2002. https://doi.org/10.1016/S0141-3910(02)00130-1.
22. Yang Y, Díaz Palencia JL, Wang N, Jiang Y, Wang D-Y. Nanocarbon-based flame retardant polymer nanocomposites. Molecules. 2021. https://doi.org/10.3390/molecules26154670.
23. Zeng C, Hossieny N, Zhang C, Wang B, Walsh SM. Morphology and tensile properties of PMMA carbon nanotubes nanocomposites and nanocomposites foams. Compos Sci Technol. 2013. https://doi.org/10.1016/j.compscitech.2013.03.024.
24. Gibertini E, Carosio F, Aykanat K, Accogli A, Panzeri G, Magagnin L. Silica-encapsulated red phosphorus for flame retardant treatment on textile. Surf Interfaces. 2021. https://doi.org/10.1016/j.surfin.2021.101252.
25. May R, Nygård T, Falkdalen U, Åström J, Hamre Ø, Stokke B. Paint it black: efficacy of increased wind turbine rotor blade visibility to reduce avian fatalities. Ecol Evol. 2020. https://doi.org/10.1002/ece3.6592.
26. Battig A, Fadul NA-R, Frasca D, Schulze D, Schartel B. Multifunctional graphene nanofiller in flame retarded polybutadiene/chloroprene/carbon black composites. e-Polymers. 2021; https://doi.org/10.1515/epoly-2021-0026
27. Kanan C, Cottrell GW. Color-to-grayscale: does the method matter in image recognition? PLoS ONE. 2012. https://doi.org/10.1371/journal.pone.0029740.
28. Gojny FH, Wichmann MHG, Fiedler B, Schulte K. Influence of different carbon nanotubes on the mechanical properties of epoxy matrix composites – a comparative study. Compos Sci Technol. 2005. https://doi.org/10.1016/j.compscitech.2005.04.021.
29. Rostam S, Mustafa DMT, Aziz SB. Investigation of flexural and creep behavior of epoxy-based nano-sized CaTiO3 particles. Results Mater. 2021. https://doi.org/10.1016/j.rinma.2020.100164.
30. Szeluga U, Kumanek B, Trzebicka B. Synergy in hybrid polymer/nanocarbon composites. A review. Compos Part A Appl Sci Manuf. 2015. https://doi.org/10.1016/j.compositesa.2015.02.021.
31. Szolnoki B, Bocz K, Sóti PL, Bodzay B, Zimonyi E, Toldy A, et al. Development of natural fibre reinforced flame retarded epoxy resin composites. Polym Degrad Stab. 2015. https://doi.org/10.1016/j.polymdegradstab.2015.04.028.
32. Kumar R, Nayak SK. Fabrication of high thermal conductive epoxy composite by adding hybrid of expanded graphite, iron (III) oxide, and silver flakes. J Mater Sci Mater Electron. 2020. https://doi.org/10.1007/s10854-020-04163-3.
33. Liu B-W, Zhao H-B, Wang Y-Z. Advanced flame-retardant methods for polymeric materials. Adv Mater. 2022. https://doi.org/10.1002/adma.202107905.
34. Taib MNAM, Antov P, Savov V, Fatriasari W, Madyaratri EW, Wirawan R, et al. Current progress of biopolymer-based flame retardant. Polym Degrad Stabil. 2022. https://doi.org/10.1016/j.polymdegradstab.2022.110153.
35. Schartel B, Hull TR. Development of fire-retarded materials—interpretation of cone calorimeter data. Fire Mater. 2007. https://doi.org/10.1002/fam.949.
36. Müller P, Schartel B. Melamine poly(metal phosphates) as flame retardant in epoxy resin: performance, modes of action, and synergy. J Appl Polym Sci. 2016. https://doi.org/10.1002/app.43549.
37. Nabipour H, Wang X, Song L, Hu Y. Metal-organic frameworks for flame retardant polymers application: a critical review. Compos Part A Appl Sci Manuf. 2020. https://doi.org/10.1016/j.compositesa.2020.106113.
38. Hakkarainen T, Mikkola E, Laperre J, Gensous F, Fardell P, Tallec Y, et al. Smoke gas analysis by Fourier Transform Infrared Spectroscopy – Summary of the SAFIR project results. Fire Mater. 2000. https://doi.org/10.1002/1099-1018(200003/04)24:23.3.CO;2-U.
39. Yang S, Wang J, Huo S, Wang M, Wang J, Zhang B. Synergistic flame-retardant effect of expandable graphite and phosphorus-containing compounds for epoxy resin: strong bonding of different carbon residues. Polym Degrad Stabil. 2016. https://doi.org/10.1016/j.polymdegradstab.2016.03.017.
40. Alamdari S, Sasani Ghamsari M, Lee C, Han W, Park H-H, Tafreshi MJ, et al. Preparation and characterization of Zinc Oxide nanoparticles using leaf extract of *Sambucus ebulus*. Appl Sci. 2020. https://doi.org/10.3390/app10103620.
41. Toldy A, Szabó A, Novák Cs, Madarász J, Tóth A, Marosi Gy. Intrinsically flame retardant epoxy resin – fire performance and

background – Part II. Polym Degrad Stab. 2008. https://doi.org/10.1016/j.polymdegradstab.2008.02.011.
42. Lee J, Park E, Subramaniam NG, Lee J, Lee J, Lee J, et al. Non-metallic element (chlorine) doped Zinc oxide grown by pulsed laser deposition for application in transparent electrode. Curr Appl Phys. 2012. https://doi.org/10.1016/j.cap.2012.05.019.

Publisher's Note Springer Nature remains neutral with regard to jurisdictional claims in published maps and institutional affiliations.

Authors and Affiliations

Péter Csvila[1] · Zsófia Kovács[1,2] · Andrea Toldy[1,2] · Tibor Czigany[1,3]

✉ Tibor Czigany
czigany@eik.bme.hu

[1] Faculty of Mechanical Engineering, Department of Polymer Engineering, Budapest University of Technology and Economics, Muegyetem Rkp. 3, 1111 Budapest, Hungary

[2] MTA-BME Lendület Sustainable Polymers Research Group, Muegyetem Rkp. 3, 1111 Budapest, Hungary

[3] HUN-REN-BME Research Group for Composite Science and Technology, Budapest University of Technology and Economics, Muegyetem Rkp. 3, 1111 Budapest, Hungary